regulated upon either ACL suppression or acetate supplementation (Fig. 4D).

Glut4 expression was selected for further examination because it is a well-characterized determinant of adipocyte glucose consumption. The reduction in Glut4 expression was specific for ACL silencing and was not observed upon silencing of AceCS1 (Fig. 4E). Notably, other differentiation markers including aP2, adiponectin, and fatty acid synthase were expressed at equal or higher levels upon silencing of either ACL or AceCS1, indicating that the adipogenic program is successfully initiated without physiologic levels of ACL or AceCS1 (Fig. 4E and fig. S4B). Upon silencing of ACL, Glut4 expression could be rescued in a dose-dependent manner by acetate supplementation (Fig. 4F), in concert with total histone acetylation levels (Fig. 4B). Furthermore, chromatin immunoprecipitation experiments revealed that acetylation of histones H3 and H4 at the Glut4 promoter was specifically reduced upon ACL silencing and could be rescued by acetate (Fig. 4G).

We next investigated whether the regulation of histone acetylation and Glut4 expression by ACL in differentiating adipocytes is nutrient-dependent by exposing the cells to various concentrations of glucose during differentiation. Standard medium for adipocyte differentiation contains 25 mM glucose, but 3T3-L1 cells can also differentiate at lower concentrations of glucose, although they accumulate lower amounts of lipid (32). We differentiated adipocytes in 1, 4, and 25 mM glucose and observed that they accumulated increasing amounts of lipid when exposed to higher levels of glucose, correlating with increasing Glut4 expression (fig. S4, C and D). Cells exposed to either 4 or 25 mM glucose exhibited similar increases in expression of the differentiation marker aP2, whereas 1 mM glucose resulted in lower levels of aP2 gene expression (fig. S4, C and D).

Histone acetylation was regulated during differentiation in a nutrient-dependent manner, increasing according to both glucose and acetate availability (fig. S4E). Glucose-dependent regulation of histone acetylation was dependent on ACL, whereas supraphysiologic concentrations of acetate increased histone acetylation in the presence or absence of ACL (Fig. 4H). Similarly, the expression of Glut4 and the glycolytic genes HK2, PFK-1, and LDH-A were regulated according to glucose availability, in an ACL-dependent manner (Fig. 4I). These results demonstrate that, during adipocyte differentiation, global histone acetylation is determined by glucose availability through an ACL-dependent pathway and that supraphysiologic levels of acetate can also contribute through AceCS1. Our data also suggest that nutrient-responsive histone acetylation may selectively affect the expression of genes required to reprogram intracellular metabolism to use glucose for ATP production and macromolecular synthesis.

We have demonstrated that ACL plays a critical role in determining the total amount of histone acetylation in multiple mammalian cell types. ACL-dependent production of acetyl-CoA contributes to increased histone acetylation during cellular response to growth factor stimulation and during adipocyte differentiation, both energy-intensive processes in which nuclear activity needs to be coordinated with cellular metabolic state. ACL-dependent acetylation can also contribute to the selective regulation of genes involved in glucose metabolism. Our data indicate that ACL activity is required to link growth factor–induced nutrient uptake and metabolism to the regulation of histone acetylation. Thus, it appears that histone acetylation can be dynamically regulated by physiologic changes in concentrations of acetyl-CoA produced by ACL. Our results also suggest that the current model for metabolic regulation of histone acetylation should be expanded to include not only redox regulation of deacetylases but also regulation of HATs by physiologic changes in the generation of acetyl-CoA.

References and Notes

1. S. K. Kurdistani, M. Grunstein, *Nat. Rev. Mol. Cell Biol.* **4**, 276 (2003).
2. B. Li, M. Carey, J. L. Workman, *Cell* **128**, 707 (2007).
3. D. E. Sterner, S. L. Berger, *Microbiol. Mol. Biol. Rev.* **64**, 435 (2000).
4. C. R. Brown, C. J. Kennedy, V. A. Delmar, D. J. Forbes, P. A. Silver, *Genes Dev.* **22**, 627 (2008).
5. A. L. Clayton, C. A. Hazzalin, L. C. Mahadevan, *Mol. Cell* **23**, 289 (2006).
6. R. Schneider, R. Grosschedl, *Genes Dev.* **21**, 3027 (2007).
7. M. A. Glozak, E. Seto, *Oncogene* **26**, 5420 (2007).
8. H. Y. Cohen et al., *Science* **305**, 390 (2004).
9. S. J. Lin, L. Guarente, *Curr. Opin. Cell Biol.* **15**, 241 (2003).
10. B. Schwer, E. Verdin, *Cell Metab.* **7**, 104 (2008).
11. H. Yang et al., *Cell* **130**, 1095 (2007).
12. A. Vaquero, R. Sternglanz, D. Reinberg, *Oncogene* **26**, 5505 (2007).
13. H. Takahashi, J. M. McCaffery, R. A. Irizarry, J. D. Boeke, *Mol. Cell* **23**, 207 (2006).
14. V. J. Starai, I. Celic, R. N. Cole, J. D. Boeke, J. C. Escalante-Semerena, *Science* **298**, 2390 (2002).
15. W. C. Hallows, S. Lee, J. M. Denu, *Proc. Natl. Acad. Sci. U.S.A.* **103**, 10230 (2006).
16. G. Hatzivassiliou et al., *Cancer Cell* **8**, 311 (2005).
17. P. L. Paine, L. C. Moore, S. B. Horowitz, *Nature* **254**, 109 (1975).
18. A. M. Bode, Z. Dong, *Nat. Rev. Cancer* **4**, 793 (2004).
19. P. S. Knoepfler et al., *EMBO J.* **25**, 2723 (2006).
20. Z. Nagy, L. Tora, *Oncogene* **26**, 5341 (2007).
21. K. L. Rice, I. Hormaeche, J. D. Licht, *Oncogene* **26**, 6697 (2007).
22. A. S. Alberts, O. Geneste, R. Treisman, *Cell* **92**, 475 (1998).
23. J. M. Sun, H. Y. Chen, J. R. Davie, *J. Biol. Chem.* **276**, 49435 (2001).
24. O. Knosp, H. Talasz, B. Puschendorf, *Mol. Cell. Biochem.* **101**, 51 (1991).
25. E. J. Yoo, J. J. Chung, S. S. Choe, K. H. Kim, J. B. Kim, *J. Biol. Chem.* **281**, 6608 (2006).
26. V. Shukla, T. Vaissiere, Z. Herceg, *Mutat. Res.* **637**, 1 (2008).
27. W. Zhang, J. R. Bone, D. G. Edmondson, B. M. Turner, S. Y. Roth, *EMBO J.* **17**, 3155 (1998).
28. P. C. Megee, B. A. Morgan, M. M. Smith, *Genes Dev.* **9**, 1716 (1995).
29. R. E. Sobel, R. G. Cook, C. A. Perry, A. T. Annunziato, C. D. Allis, *Proc. Natl. Acad. Sci. U.S.A.* **92**, 1237 (1995).
30. C. B. Thompson, P. B. Challoner, P. E. Neiman, M. Groudine, *Nature* **319**, 374 (1986).
31. A. Johnsson, Y. Xue-Franzen, M. Lundin, A. P. Wright, *Eukaryot. Cell* **5**, 1337 (2006).
32. Y. Lin et al., *J. Biol. Chem.* **280**, 4617 (2005).
33. Materials and methods are available as supporting material on *Science* Online.
34. We thank members of the Thompson laboratory for helpful comments and discussion and A. Stout for assistance with the deconvolution microscopy. Supported by grants to C.B.T. from NIH and the National Cancer Institute. K.E.W. is a Damon Runyon Fellow supported by the Damon Runyon Cancer Research Foundation, DRG-1955-07. U.M.S. is supported in part by a training grant from NIH, T32-HL07439-27.

Phasic Firing in Dopaminergic Neurons Is Sufficient for Behavioral Conditioning

Hsing-Chen Tsai,[1,2]* Feng Zhang,[2]* Antoine Adamantidis,[3] Garret D. Stuber,[4] Antonello Bonci,[4] Luis de Lecea,[3] Karl Deisseroth[2,3]†

Natural rewards and drugs of abuse can alter dopamine signaling, and ventral tegmental area (VTA) dopaminergic neurons are known to fire action potentials tonically or phasically under different behavioral conditions. However, without technology to control specific neurons with appropriate temporal precision in freely behaving mammals, the causal role of these action potential patterns in driving behavioral changes has been unclear. We used optogenetic tools to selectively stimulate VTA dopaminergic neuron action potential firing in freely behaving mammals. We found that phasic activation of these neurons was sufficient to drive behavioral conditioning and elicited dopamine transients with magnitudes not achieved by longer, lower-frequency spiking. These results demonstrate that phasic dopaminergic activity is sufficient to mediate mammalian behavioral conditioning.

Dopaminergic (DA) neurons have been suggested to be involved in the cognitive and hedonic underpinnings of motivated behaviors (1–4). Changes in the firing pattern of DA neurons between low-frequency tonic activity and phasic bursts of action potentials could encode reward prediction errors and incentive salience (5). Consistent with the reward prediction-error hypothesis, DA neuron firing activity is depressed by aversive stimuli (6).

However, it remains unclear whether DA neuron activation alone is sufficient to elicit reward-related behaviors. Lesion, electrical stimulation, and psychopharmacology studies have been important but have not allowed causal and temporally precise control of DA neurons in freely moving mammals; for example, electrical stimulation inevitably activates multiple classes of neurons within heterogeneous brain tissue, and pharmacological stimulation does not allow delivery of defined patterns of DA neuron spikes in vivo.

To control DA neurons selectively, we used a Cre-inducible adeno-associated virus (AAV) vector (7, 8) carrying the gene encoding the light-activated cation channel channelrhodopsin-2 (ChR2) in-frame fused to enhanced yellow fluorescent protein (ChR2-EYFP) (9–11). To ensure that there would be no substantial expression leak in nontargeted cell types, we designed the Cre-inducible AAV vector with a double-floxed inverted open reading frame (ORF), wherein the ChR2-EYFP sequence is present in the antisense orientation (Fig. 1A). Stereotactic delivery of this vector into the VTA of tyrosine hydrox-

ylase (TH):: internal ribosomal entry site (IRES)–Cre transgenic mice enables DA neuron-specific expression of ChR2-EYFP. Upon transduction, Cre-expressing TH cells invert the ChR2-EYFP ORF in irreversible fashion and thereby activate sustained ChR2-EYFP expression under the strong, constitutively active elongation factor 1α (EF-1α) promoter.

We validated the specificity and efficacy of this targeting strategy in vivo. In coronal VTA sections of transduced TH::IRES-Cre brains, ChR2-EYFP specifically co-localized with endogenous TH (Fig. 1B). Greater than 90% of TH-immunopositive cells were positive for ChR2-EYFP near virus injection sites, and more than 50% were positive overall, demonstrating highly efficacious transduction of the TH cells. Of ChR2-EYFP–expressing cells, $98.3 \pm 0.5\%$ were co-labeled by TH staining (Fig. 1C), demonstrating high specificity. Expression was stable and persistent for at least 2 months, and ChR2-EYFP–expressing neurons displayed robust projections; EYFP-positive fibers richly innervated local neurons in downstream nucleus accumbens (NAc) (Fig. 1D) (12).

To assess the potential for optogenetic control of transduced cells, we used whole-cell patch clamps to measure light-induced membrane currents in ChR2-expressing DA neurons (Fig. 2A). ChR2-EYFP–expressing cells in the VTA displayed typical electrophysiological properties of DA neurons with a mean resting membrane potential of -56.0 ± 1.8 mV and a mean membrane resistance of 372.3 ± 19.3 megohm ($n = 10$ cells), consistent with previously reported values for VTA DA neurons (13) and indicating that expression of ChR2 alone does not affect their basic physiology. Under blue light (473 nm) illumination, all patched

cells exhibited prominent inward photocurrents (Fig. 2, B and C; $n = 10$ cells). Trains of light flashes drove action potential firing in ChR2-EYFP neurons; with use of low- and high-frequency light trains, we evoked tonic and phasic DA neuron firing, respectively (Fig. 2D). DA neurons typically do not maintain high-frequency spiking (14); 1- to 5-Hz light pulses drove long DA neuron spike trains reliably, whereas bursting at 20 Hz or greater for prolonged trains evoked action potentials in <50% of light pulses (Fig. 2E and fig. S1; bursts maintaining the >15-Hz spiking characteristic of phasic firing could be elicited simply by using higher-frequency light pulse trains). Optrode recording confirmed that optical stimulation of VTA DA neurons in vivo evoked broad spike waveforms consistent with extracellular waveforms for VTA DA neurons (6) (Fig. 2F and fig. S2).

We next tested the behavioral conditioning effects of phasic DA neuron activity via the conditioned place preference (CPP) paradigm (Fig. 3A and fig. S3), with use of phasic optogenetic stimulation (15) of DA neurons as our conditioning stimuli (Fig. 3, B and C). As a control, we paired the opposite chamber with the same number of light pulses delivered instead at 1 Hz. Mice were subjected to 2 days of conditioning, and conditioned preference was determined by comparing time spent in each chamber of the apparatus. In the first round of experiments, mice received phasic (50-Hz optical stimulation) conditioning in one chamber on the first day of conditioning (day 2), and 1-Hz optical stimulation in the other chamber on the second day of conditioning (day 3); two cohorts of mice were used with the chamber-stimulation pairing reversed to control for spontaneous preference shifts (fig. S3). Mice developed a clear place

[1]Neuroscience Program, W080 Clark Center, 318 Campus Drive West, Stanford University, Stanford, CA 94305, USA. [2]Department of Bioengineering, W083 Clark Center, 318 Campus Drive West, Stanford University, Stanford, CA 94305, USA. [3]Department of Psychiatry and Behavioral Sciences, W083 Clark Center, 318 Campus Drive West, Stanford University, Stanford, CA 94305, USA. [4]Ernest Gallo Clinic and Research Center, Department of Neurology, Wheeler Center for the Neurobiology of Drug Addiction, University of California San Francisco, San Francisco, CA 94158, USA.

*These authors contributed equally to this work.
†To whom correspondence should be addressed. E-mail: deissero@stanford.edu

Fig. 1. Specific ChR2 expression in DA neurons. (**A**) Schematic of the Cre-dependent AAV; the gene of interest is doubly flanked by two sets of incompatible lox sites. Upon delivery into TH::IRES-Cre transgenics, ChR2-EYFP is inverted to enable transcription from the EF-1α promoter. (**B**) Confocal images showing cell-specific ChR2-EYFP expression (green) in TH neurons (red). (**C**) Statistics of expression in TH neurons ($n = 491$); error bars represent SEM throughout. (**D**) Labeled VTA DA neurons project to downstream brain regions; confocal images of ChR2-EYFP–positive axons (green) innervating target neurons in NAc (NeuN, red).
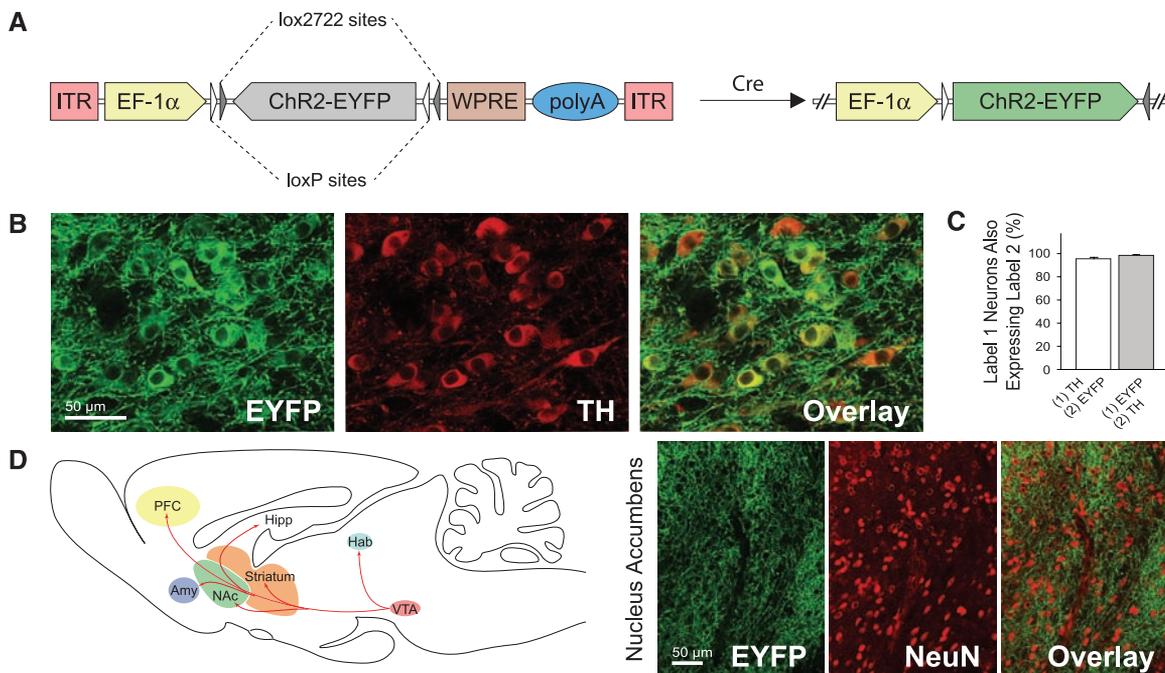
Fig. 2. Photoactivation of DA neurons in intact tissue. (**A**) Recording from transduced neurons in acute VTA slices. Recorded neurons are verified by intracellular dye loading (ChR2-EYFP, green; AlexaFluor 594, red). (**B**) Continuous blue light (473 nm) evokes inward photocurrents. (**C**) Summary of photocurrent properties ($n = 10$). (**D**) Whole-cell recording of DA neurons showing spontaneous activity and tonic and phasic firing evoked by 1-Hz and 50-Hz light flash trains, respectively (25 flashes, 15 ms per flash). (**E**) Light-evoked spike trains are reliable over a range of frequencies; percentage of action potentials evoked by 25 light flashes at indicated frequencies (1 to 50 Hz) is shown ($n = 7$). (**F**) In vivo optrode recording of VTA DA neurons in a transduced TH::IRES-Cre anesthetized mouse showing light-evoked DA spikes; see fig. S2. (Inset) Typical triphasic DA extracellular spike.
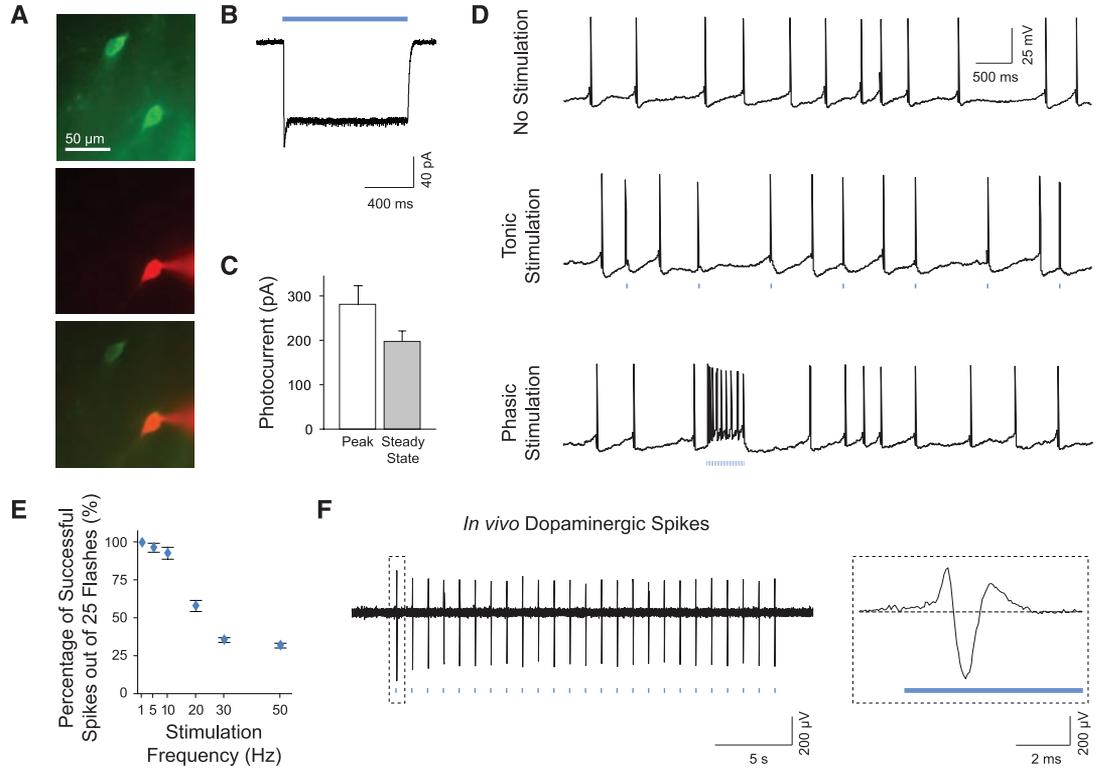
Fig. 3. Photoactivation of DA neurons induces place preference. (**A**) CPP timeline (see also fig. S3). (**B**) Light delivery parameters; 25 flashes at 1 or 50 Hz were delivered with a periodicity of 1 min. (**C**) Optical fiber is inserted through a cannula guide implanted over the VTA to photoactivate DA neurons. (**D**) Representative density maps showing conditioned preference; pseudocolor represents duration at each position. (**E**) Conditioning effect of DA neuron modulation. (Left) Comparison of time in each chamber during pretest (white) and posttest (gray). (Right) Comparison of preference scores for experimental (Phasic Stim, $n = 13$) and control cohorts (No Stim Control, $n = 9$; Littermate Control, $n = 9$). n.s. indicates not significant, $*P < 0.05$, $**P < 0.01$, and $***P < 0.001$. (**F**) Difference scores (calculated as the difference between time spent during pre- and posttest in the specified chamber) for each chamber shows a statistically significant shift in place preference. (**G**) Analysis of anxiety (fractional time in center of a chamber; $n = 13$). (**H**) Chamber entries, long-range locomotion (different sequential beam breaks), and short-range locomotion (repeated break of the same beam) during pre- and posttest ($n = 13$).
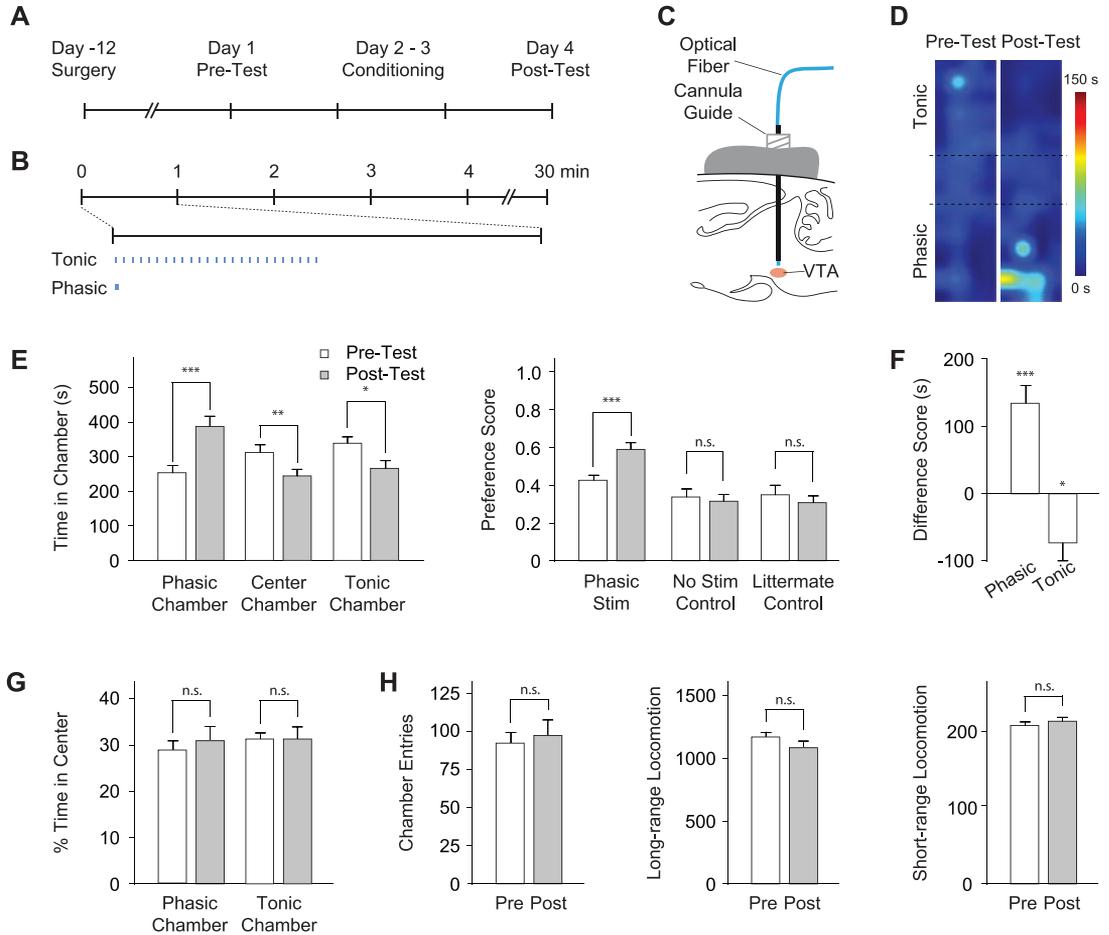
preference for the chamber associated with phasic optical stimulation by several measures (Fig. 3, D to F; $P < 0.001$ by Student's t test; $n = 13$ mice), and both cohorts of mice exhibited this conditioned preference independent of chamber pairing (fig. S5).

We performed two classes of control experiments to validate the results. First, nontransgenic littermates ($n = 9$) were injected with Cre-dependent ChR2-EYFP AAV and subjected to the same stimulation paradigm as the experimental animals. Separately, TH::IRES-Cre transgenic mice ($n = 9$) were injected with Cre-dependent ChR2-EYFP AAV but received no optical stimulation during conditioning to further control for spontaneous preference shifts. Neither control group showed a significant CPP (Fig. 3E right, $P > 0.5$ by Student's t test). Furthermore, we did not find any significant changes in anxiety-related behaviors (Fig. 3G) or in locomotor activity (Fig. 3H) during preference tests and in open field tests (fig. S6).

Next, we tested whether the CPP effect observed was due to an appetitive effect from 50-Hz stimulation or to an aversive effect from 1-Hz stimulation. We compared the effect of each firing modality with no stimulation in two independent cohorts. Consistent with the previous CPP experiments (Fig. 3, E and F), the phasic cohort displayed significant place preference for the stimulation chamber after conditioning (Fig. 4, A and C), from 251 ± 28 s during pretest to 522 ± 63s during posttest ($n = 7$ mice; $P < 0.05$, Student's t test). However, the 1-Hz cohort ($n = 6$) showed no place aversion for the 1-Hz stimulation chamber (showing a trend toward place preference for 1 Hz instead; Fig. 4, B and C). We hypothesized that the CPP effect observed for the phasic cohort could be due to larger transient DA release triggered by the 50-Hz optical stimulation. We therefore used in vivo fast-scan cyclic voltammetry (FSCV) (16, 17) to detect DA transients. Maintaining the optical fiber in the VTA, we implanted a carbon fiber electrode for measuring DA signals in the NAc, one of the major targets of VTA DA projections (Fig. 1D). Despite sharing the same total illumination duration and number of light flashes (25 15-ms light flashes at 1 Hz or 50 Hz), the 50-Hz light train elicited larger DA transients (Fig. 4, D and E). Indeed, the mean peak DA transient concentrations in the NAc were measured at 75.9 ± 24.5 nM and 1.3 ± 0.8 nM, respectively, for the 50-Hz and 1-Hz stimuli (Fig. 4E);

the former is similar to the magnitude of natural reward-triggered dopamine transients (16), whereas DA accumulation during chronic 1-Hz stimulation remained much lower (fig. S7; this level of DA could still theoretically contribute to behavioral changes).

Rodents learn to associate the effects of stimuli with their environment and subsequently display a conditioned place preference for that environment (18). Previous studies have demonstrated the important role of DA in the processing of salient signals (19) and goal-directed behaviors (20). However, it has been unclear whether other circuits and neurotransmitter systems are required at the same time (21) and whether specific patterns of activity in distinct neuron types are sufficient to effect place preference. To enable direct testing of the role of phasic DA neuron firing on behavioral conditioning, we developed a versatile Cre-inducible gene expression system to decouple the strength of transgene expression from cell type–specific promoters (which are often too weak to drive functional expression of opsins). By using this system, we selectively modulated DA neuron activity with defined stimulation patterns in the CPP paradigm and found that phasic stimulation suf-
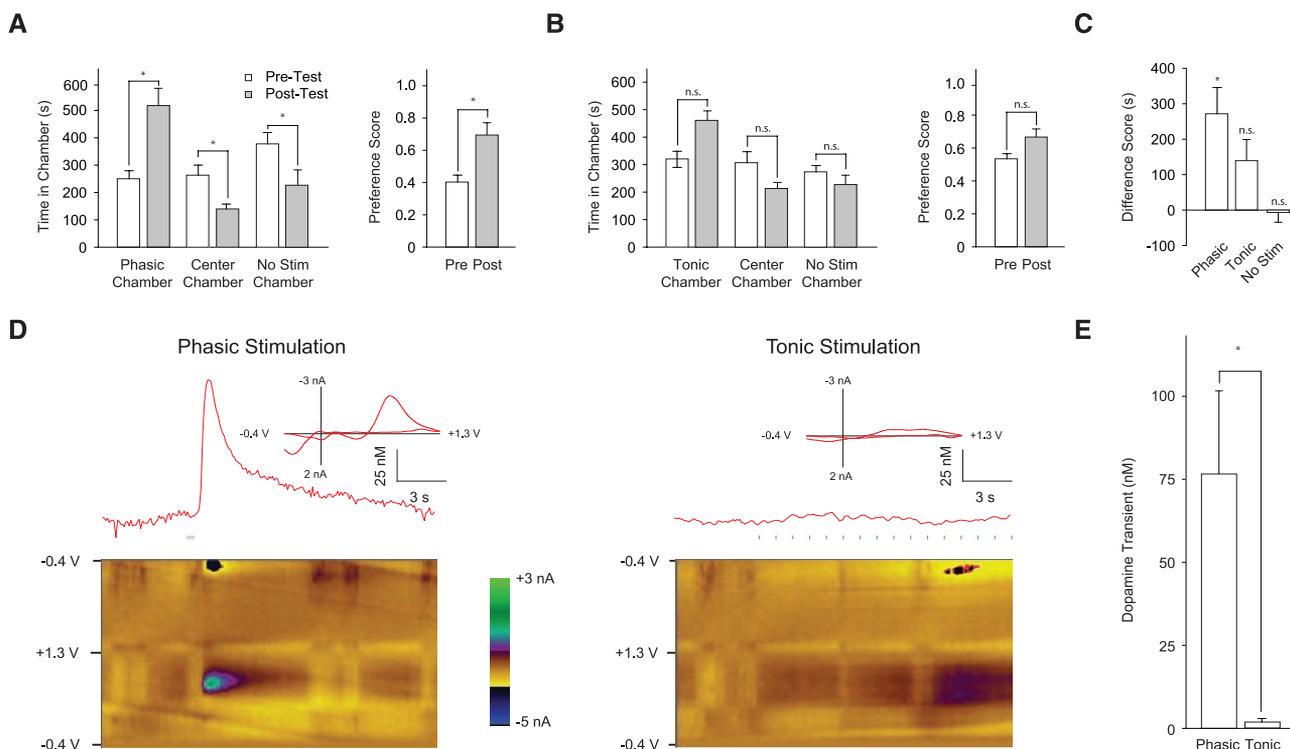
Fig. 4. Phasic DA neuron stimulation leads to transient DA release and place preference. (**A** and **B**) Effect of phasic (50 Hz) (A) and tonic (1 Hz) (B) stimulation on place preference. (Left) Time spent in each chamber during preference test. (Right) Comparison of preference scores; for A, $n = 7$, and for B, $n = 6$. *$P < 0.05$. (**C**) Relative effects of stimulation frequency examined by using the difference scores for phasic, tonic, and nonassociative control (same as No Stim in Fig. 3E) cohorts. (**D**) FSCV measurements of VTA stimulation–triggered transient DA release in NAc in anesthetized TH::IRES-Cre mice. (Top) Representative voltammetry traces during phasic (25 flashes per 50 Hz) and tonic (16 flashes per 1 Hz) stimulation of VTA. (Insets) Background-subtracted voltammogram taken from the peak of stimulation, indicating that signal measured is DA on the basis of comparison to voltammograms of DA obtained in vitro. (Bottom) All background-subtracted voltammograms recorded over the 20-s interval. y axis is applied potential (E_{apps} versus Ag/AgCl reference electrode); x axis is the time at which each voltammogram was recorded. Current changes at the electrode are encoded in color. DA can be seen during stimulation at the feature ~0.650 V (oxidation peak encoded as green) and between ~−0.20 V and ~−0.25 V at the end of the voltage scan. (**E**) Comparison of phasic and tonic light-evoked DA transients ($n = 3$).

ficed to establish place preference in the absence of other reward. These results establish a causal role in behavioral conditioning for defined spiking modes in a specific cell type; of course, even a single cell type can release multiple neurotransmitters and neuromodulators (for example, VTA DA neurons primarily release DA but can also release other neurotransmitters such as glutamate) and will exert effects through multiple distinct downstream cell types. Indeed, the optogenetic approach, integrated with electrophysiological, behavioral, and electrochemical readout methods, opens the door to exploring the causal, temporally precise, and behaviorally relevant interactions of DA neurons with other neuromodulatory circuits (22–25), including monoaminergic and opioid circuits important in neuropsychiatric illnesses (26–28). In the process of identifying candidate interacting neurotransmitter systems, downstream neural circuit effectors (29), and subcellular biochemical mechanisms on time scales appropriate to behavior and relevant circuit dynamics, it will be important to continue to leverage the specificity and temporal precision of optogenetic control (30).

References and Notes

1. R. A. Wise, *Nat. Rev. Neurosci.* **5**, 483 (2004).
2. B. J. Everitt, T. W. Robbins, *Nat. Neurosci.* **8**, 1481 (2005).
3. T. E. Robinson, K. C. Berridge, *Brain Res. Brain Res. Rev.* **18**, 247 (1993).
4. G. F. Koob, M. Le Moal, *Science* **278**, 52 (1997).
5. W. Schultz, *Annu. Rev. Neurosci.* **30**, 259 (2007).
6. M. A. Ungless, P. J. Magill, J. P. Bolam, *Science* **303**, 2040 (2004).
7. F. Zhang, Larry C. Katz Memorial Lecture presented at the Cold Spring Harbor Laboratory Meeting on Neuronal Circuits, Cold Spring Harbor, NY, 13 to 16 March 2008.
8. D. Atasoy, Y. Aponte, H. H. Su, S. M. Sternson, *J. Neurosci.* **28**, 7025 (2008).
9. E. S. Boyden, F. Zhang, E. Bamberg, G. Nagel, K. Deisseroth, *Nat. Neurosci.* **8**, 1263 (2005).
10. G. Nagel *et al.*, *Proc. Natl. Acad. Sci. U.S.A.* **100**, 13940 (2003).
11. Materials and methods are available as supporting material on *Science* Online.
12. A. Bjorklund, S. B. Dunnett, *Trends Neurosci.* **30**, 194 (2007).
13. Q. S. Liu, L. Pu, M. M. Poo, *Nature* **437**, 1027 (2005).
14. S. Robinson, D. M. Smith, S. J. Mizumori, R. D. Palmiter, *Proc. Natl. Acad. Sci. U.S.A.* **101**, 13329 (2004).
15. A. R. Adamantidis, F. Zhang, A. M. Aravanis, K. Deisseroth, L. de Lecea, *Nature* **450**, 420 (2007).
16. P. E. Phillips, G. D. Stuber, M. L. Heien, R. M. Wightman, R. M. Carelli, *Nature* **422**, 614 (2003).
17. G. D. Stuber *et al.*, *Science* **321**, 1690 (2008).
18. T. M. Tzschentke, *Addict. Biol.* **12**, 227 (2007).
19. C. M. Cannon, R. D. Palmiter, *J. Neurosci.* **23**, 10827 (2003).
20. A. A. Grace, S. B. Floresco, Y. Goto, D. J. Lodge, *Trends Neurosci.* **30**, 220 (2007).
21. T. S. Hnasko, B. N. Sotak, R. D. Palmiter, *J. Neurosci.* **27**, 12484 (2007).
22. P. W. Kalivas, *Am. J. Addict.* **16**, 71 (2007).
23. M. R. Picciotto, W. A. Corrigall, *J. Neurosci.* **22**, 3338 (2002).
24. J. A. Dani, D. Bertrand, *Annu. Rev. Pharmacol. Toxicol.* **47**, 699 (2007).
25. G. C. Harris, G. Aston-Jones, *Neuropsychopharmacology* **28**, 865 (2003).
26. E. J. Nestler, W. A. Carlezon Jr., *Biol. Psychiatry* **59**, 1151 (2006).
27. J. Williams, P. Dayan, *J. Child Adolesc. Psychopharmacol.* **15**, 160 (2005).
28. A. M. Graybiel, *Annu. Rev. Neurosci.* **31**, 359 (2008).
29. W. Shen, M. Flajolet, P. Greengard, D. J. Surmeier, *Science* **321**, 848 (2008).
30. F. Zhang *et al.*, *Nature* **446**, 633 (2007).
31. We thank M. Wightman, P. Phillips, and the entire Deisseroth laboratory for their support. All reagents and protocols are freely distributed and supported by the authors (www.optogenetics.org); because these tools are not protected by patents, Stanford University has applied for a patent to ensure perpetual free distribution to the international academic nonprofit community. H.C.T. is supported by a Stanford Graduate Fellowship. F.Z. and G.D.S. are supported by NIH National Research Service award. A.R.A. is supported by the Fonds National de la Recherche Scientifique, NARSAD, and the Fondation Leon Fredericq. L.d.L. is supported by National Institute on Drug Abuse (NIDA), Defense Advanced Research Projects Agency, and NARSAD. K.D. is supported by NSF; National Institute of Mental Health; NIDA; and the McKnight, Coulter, Snyder, Albert Yu and Mary Bechmann, and Keck foundations.

The Human K-Complex Represents an Isolated Cortical Down-State

Sydney S. Cash,[1]*† Eric Halgren,[2]* Nima Dehghani,[2] Andrea O. Rossetti,[5] Thomas Thesen,[3] ChunMao Wang,[3] Orrin Devinsky,[3] Ruben Kuzniecky,[3] Werner Doyle,[3] Joseph R. Madsen,[4] Edward Bromfield,[5] Loránd Erőss,[6] Péter Halász,[7,9] George Karmos,[8,9] Richárd Csercsa,[8] Lucia Wittner,[6,8] István Ulbert[6,8,9]*

The electroencephalogram (EEG) is a mainstay of clinical neurology and is tightly correlated with brain function, but the specific currents generating human EEG elements remain poorly specified because of a lack of microphysiological recordings. The largest event in healthy human EEGs is the K-complex (KC), which occurs in slow-wave sleep. Here, we show that KCs are generated in widespread cortical areas by outward dendritic currents in the middle and upper cortical layers, accompanied by decreased broadband EEG power and decreased neuronal firing, which demonstrate a steep decline in network activity. Thus, KCs are isolated "down-states," a fundamental cortico-thalamic processing mode already characterized in animals. This correspondence is compatible with proposed contributions of the KC to sleep preservation and memory consolidation.

Although the electroencephalogram (EEG) is known to directly and instantaneously reflect synaptic and active transmembrane neuronal currents, the specific channels, synapses, and circuits that generate particular EEG elements in humans remain poorly specified. Much of the EEG is composed of repeated wave forms with characteristic morphologies, durations, amplitudes, frequency content, evoking events, and background states (1). The largest of these EEG "graphoelements" is the KC, characterized by a short surface-positive transient followed by a

slower, larger surface-negative complex with peaks at 350 and 550 ms, and then a final positivity peaking near 900 ms, followed sometimes by 10- to 14-Hz "spindles" (2–4). KCs occur in non–rapid-eye-movement (non-REM) sleep, especially stage 2. Deeper sleep (stages 3 to 4) is characterized by slow waves, demonstrated in extensive animal studies to consist of a "slow oscillation" between periods of intense firing by both excitatory and inhibitory cortical neurons (termed "up-states") and periods of neuronal silence ("down-states") (5–9). Using micro- and

macro-electrode arrays placed in patients undergoing evaluation for epilepsy (10), we demonstrate that the microphysiological characteristics of human KCs appear identical to those of down-states recorded in the same patients.

Typical KCs were recorded in eight patients (11). KCs were either spontaneous or evoked by a weak auditory stimulus. Within a given patient, the basic KC wave forms were similar regardless of whether they were recorded at the scalp or intracranially (Fig. 1A). In all cases, the wave form was dominated by a large deflection occurring ~500 to 600 ms after the onset of a stimulus, or after the onset of the initial deflection for spontaneous KCs. Characteristic KC wave forms were recorded by subdural electrodes placed on all cortical lobes, demonstrating widespread

[1]Department of Neurology, Epilepsy Division, Massachusetts General Hospital, Harvard Medical School, Boston, MA 02114, USA. [2]Departments of Radiology, Neurosciences, and Psychiatry, University of California at San Diego, San Diego, CA 92093, USA. [3]Comprehensive Epilepsy Center, New York University School of Medicine, New York, NY 10016, USA. [4]The Children's Hospital, Boston, MA 02115, USA. [5]Brigham and Women's Hospital, Boston, MA 02115, USA. [6]National Institute of Neurosurgery, H-1145 Budapest, Hungary. [7]National Institute of Psychiatry and Neurology, Epilepsy Center, H-1145 Budapest, Hungary. [8]Institute for Psychology, Hungarian Academy of Sciences, H-1394 Budapest, Hungary. [9]Péter Pázmány Catholic University, Department of Information Technology, H-1083 Budapest, Hungary.

*These authors contributed equally to this work.
†To whom correspondence should be addressed. E-mail: scash@partners.org